Journal of Science and Transport Technology

University of Transport Technology

Nonlinear buckling and postbuckling of spiral stiffened FG-GPLRC cylindrical shells subjected to torsional loads

Le Kha Hoa[1], Vu Tho Hung[2], Pham Hong Quan[3], Vu Hoai Nam[2,*]

[1]Military Academy of Logistics, Hanoi 100000, Vietnam
[2]University of Transport Technology, Hanoi 100000, Vietnam
[3]University of Transport Technology, Vinh Phuc 280000, Vietnam

Article info
*Corresponding author:
E-mail address:
hoainam.vu@utt.edu.vn

Received: 06 October 2021
Accepted: 18 November 2021
Published: 25 November 2021

Abstract: The nonlinear buckling behavior of functionally graded graphene platelet reinforced composite (FG-GPLRC) cylindrical shells reinforced by ring, stringer and/or spiral FG-GPLRC stiffeners under torsional loads is studied by an analytical approach. The governing equations are based on the Donnell shell theory with geometrical nonlinearity of von Kármán-Donnell-type, combining the improvability of Lekhnitskii's smeared stiffeners technique for spiral FG-GPLRC stiffeners. The effects of mechanical and thermal loads are considered in this paper. The number of spiral stiffeners, stiffener angle, and graphene volume fraction, are numerically investigated. A very large effect of spiral FG-GPLRC stiffeners on the nonlinear buckling behavior of shells in comparison with orthogonal FG-GPLRC stiffeners is approved in numerical results.

Keywords: Functionally graded graphene platelet reinforced composite (FG-GPLRC); Spiral stiffener; Nonlinear buckling; Torsional load; Cylindrical shell

1. Introduction

The circular cylindrical shell is the typical structure of revolution shells. Due to the closed circumferential condition, the thermo-mechanical behavior of these structures is complex. The linear and nonlinear buckling investigations of cylindrical shells made from classical and modern materials have been the interesting matters for the researcher in the world, where, the torsionally loaded problems are the difficult and exciting problems.

The stability and vibration responses of isotropic and functionally graded (FGM) cylindrical shells under torsional loads were investigated and discussed in a relatively comprehensive way by many authors [1-10]. Recently, the nonlinear torsional postbuckling behavior of FGM cylindrical shells reinforced by homogeneous or FGM spiral stiffeners was also studied and showed the special effects of spiral stiffened reinforcement on the thermo-mechanical behavior of shells [8-10]. The significant effects of spiral stiffeners were also validated in the case of axially loaded FGM cylindrical shells [11] taking into account the thermal environment. Additionally, another type of revolution shell as a toroidal shell segment was mentioned by Phuong et al. [12] in the case of functionally graded graphene-reinforced composite laminated structures subjected to external pressure.

Graphene is known to be a metamaterial

with extraordinary thermo-mechanical properties. Options for reinforcing graphene into thin-walled structures are increasingly popular to create different types of advanced materials. By reinforcing graphene platelet into an isotropic matrix for a thin-walled structure with the fraction of the volume of graphene changing piecewisely through each thin layer, the material properties of the resulting composite are moderately smooth and continuous throughout the thickness of the structure. The new composite is called with the international name as Functionally graded graphene platelet reinforced composite (FG-GPLRC) [13-15]. The stability, bending and dynamic responses of FG-GPLRC plates subjected to static, dynamic, and thermal loads also were studied and evaluated.

A special option of reinforcement design for FG-GPLRC cylindrical shells is proposed in this present report. The shells can be stiffened by orthogonal or spiral FG-GPLRC stiffeners with the suitable distribution law of graphene platelet. An improved smeared stiffener technique is developed for FG-GPLRC stiffeners and isapplied to the analytical approach. The nonlinear buckling analysis of stiffened FG-GPLRC cylindrical shells subjected to torsional loads is studied and evaluated. The prebuckling and linear and nonlinear postbuckling states are taken into account, and the Galerkin procedure is utilized. The effects of orthogonal and spiral FG-GPLRC stiffeners, including the volume fraction of graphene platelet, distribution laws on the torsional postbuckling behavior of FG-GPLRC cylindrical shells are compared and evaluated.

2. Theoretical formulations and solution of problem

The considered FG-GPLRC thin cylindrical shells in this paper are investigated with the torsional load τ, the length L in the longitudinal direction, the radius R measured to the mid-plane of shell, and the thickness h included many layers. The quasi-Cartesian coordinate system of shell and other parameters of shells and stiffeners can be recognized in Fig 1. Considering that the FG-GPLRC shell is stiffened by the closely spaced ring and stringer or spiral FG-GPLRC stiffeners at the inside surface of the cylindrical shell. The continuous condition of stiffener design between shell and stiffener system can be satisfied if the stiffeners are made by FG-GPLRC with the selected distribution law of graphene platelet.

The proposed design of this paper is that the shell skin and stiffeners have the same graphene platelet volume fraction at the connect plane. Three shell skin-stiffener connected types are considered as UD, FG-X, FG-O GPLRC shell skin are stiffened by UD, FG-X, FG-O GPLRC stiffeners, respectively (see Fig 1).

FG-GPLRC cylindrical shells with a large number of layers are presented in this paper. The volume fractions VGPL of graphene platelet of the kth layer for the three distribution law types are applied as

Type 1: UD-GPLRC

$$V_{GPL}^{(k)} = V_{GPL}^{*} \tag{1}$$

Type 2: FG-X

$$V_{GPL}^{(k)} = 2V_{GPL}^{*}\frac{\left|2k - N_L - 1\right|}{N_L} \tag{2}$$

Type 3: FG-O

$$V_{GPL}^{(k)} = 2V_{GPL}^{*}\left(1 - \frac{\left|2k - N_L - 1\right|}{N_L}\right) \tag{3}$$

where k = 1, 2, …N_L and N_L is the total number of layers of the structures. The total volume fraction of graphene platelet V_{GPL}^{*} can be estimated as [13-15]

$$V_{GPL}^{*} = \frac{W_{GPL}}{W_{GPL} + \left(\rho_{GPL} / \rho_m\right)\left(1 - W_{GPL}\right)} \tag{4}$$

in which ρ_{GPL} and ρ_m are the mass densities of the graphene platelet and the polymer matrix, respectively, W_{GPL} is the graphene platelet weight fraction.

The effective elastic modulus of FG-GPLRC for each layer can be predicted by using the modified Halpin-Tsai micromechanics model taking into account the nano-geometrical and

dimension effects, presented as [13-15]

$$E=\left(3\frac{1+\xi_L\eta_L V_{GPL}}{1-\eta_L V_{GPL}}+5\frac{1+\xi_T\eta_T V_{GPL}}{1-\eta_T V_{GPL}}\right)\frac{E_m}{8} \tag{5}$$

where

$$\eta_L=\frac{(E_{GPL}/E_m)-1}{(E_{GPL}/E_m)+\xi_L},\xi_L=2(a_{GPL}/t_{GPL}),$$
$$\eta_T=\frac{(E_{GPL}/E_m)-1}{(E_{GPL}/E_m)+\xi_T},\xi_T=2(b_{GPL}/t_{GPL}) \tag{6}$$

The Poisson's ratio and thermal expansion coefficient of GPLRCs, respectively, can be popularly estimated by the simple rule of mixture, listed as

$$\nu=\nu_m V_m+\nu_{GPL}V_{GPL},$$
$$\alpha=\alpha_m V_m+\alpha_{GPL}V_{GPL} \tag{7}$$

where $V_m=1-V_{GPL}$ is the volume fraction of isotropic matrix.

Stress-strain relations of Hooke's law of FG-GPLRC shell skin are applied as

$$\begin{bmatrix}\sigma_x\\ \sigma_y\\ \sigma_{xy}\end{bmatrix}=\begin{bmatrix}Q_{11}^{sh} & Q_{12}^{sh} & 0\\ Q_{12}^{sh} & Q_{22}^{sh} & 0\\ 0 & 0 & Q_{66}^{sh}\end{bmatrix}\begin{bmatrix}\varepsilon_x\\ \varepsilon_y\\ \gamma_{xy}\end{bmatrix} \tag{8}$$

where the expressions of the reduced stiffness matrix components in Eq. (8) are presented as

$$Q_{11}^{sh}=Q_{22}^{sh}=\frac{E(z)}{1-\nu(z)^2},$$
$$Q_{12}^{sh}=\frac{E(z)}{1-\nu(z)},$$
$$Q_{66}^{sh}=\frac{E(z)}{2[1+\nu(z)]}$$

Stress-strain relations of Hooke's law of FG-GPLRC stiffeners (in the local coordinate), are used by

$$\sigma_\eta^i=E_i\varepsilon_\eta,\ i=(s,r,l) \tag{9}$$

where the superscripts (s,r,l) denote the spiral, ring and longitudinal directions.

The smeared stiffeners technique is developed with the coordinate transformation technique for spiral FG-GPLRC stiffeners, while, the stress–strain relations are integrated through the thickness of the shell and stiffeners, the force and moment equations of stiffened FG-GPLRC circular cylindrical shell can be presented in the following form

$$\begin{bmatrix}N_x\\ N_y\\ N_{xy}\\ M_x\\ M_y\\ M_{xy}\end{bmatrix}=\begin{bmatrix}A_{11} & A_{12} & 0 & B_{11} & B_{12} & 0\\ A_{12} & A_{22} & 0 & B_{12} & B_{22} & 0\\ 0 & 0 & A_{66} & 0 & 0 & B_{66}\\ B_{11} & B_{12} & 0 & D_{11} & D_{12} & 0\\ B_{12} & B_{22} & 0 & D_{12} & D_{22} & 0\\ 0 & 0 & B_{66} & 0 & 0 & D_{66}\end{bmatrix}\begin{bmatrix}\varepsilon_x^0\\ \varepsilon_y^0\\ \gamma_{xy}^0\\ \chi_x\\ \chi_y\\ \chi_{xy}\end{bmatrix} \tag{10}$$

where the stiffnesses of the stiffness matrix in Eq. (10) are calculated by the sum of shell and stiffener system, as

$$(A_{ij},B_{ij},D_{ij})=(A_{ij}^{sh},B_{ij}^{sh},D_{ij}^{sh})+(\bar{A}_{ij},\bar{B}_{ij},\bar{D}_{ij}) \tag{11}$$

with the stiffnesses of the shells are determined by calculating the following integral, as

$$(A_{ij}^{sh},B_{ij}^{sh},D_{ij}^{sh})=\int_{-h/2}^{h/2}Q_{ij}^{sh}(1,z,z^2)dz \tag{12}$$

The stiffness components of stiffeners are presented after the applying of improved smeared stiffener technique, as

$$\bar{A}_{22}=\mu_1\frac{b_y}{d_y}E_1^{sy}+\mu_2 2\sin^4\theta\frac{b_l}{d_l}E_1^{sl},$$
$$\bar{A}_{66}=\mu_2 2\sin^2\theta\cos^2\theta\frac{b_l}{d_l}E_1^{sl},$$
$$\bar{B}_{22}=\mu_1\frac{b_y}{d_y}E_2^{sy}+\mu_2 2\sin^4\theta\frac{b_l}{d_l}E_2^{sl},$$
$$\bar{B}_{66}=\mu_2 2\sin^2\theta\cos^2\theta\frac{b_l}{d_l}E_2^{sl},$$
$$\bar{D}_{11}=\mu_1\frac{b_x}{d_x}E_3^{sx}+\mu_2 2\cos^4\theta\frac{b_l}{d_l}E_3^{sl}, \tag{13}$$

$$\bar{D}_{12} = \mu_2 2\sin^2\theta\cos^2\theta\frac{b_l}{d_l}E_3^{sl},$$

where

$$\left(E_1^{si}, E_2^{si}, E_3^{si}\right) = \int_{\Omega} E(z)(1, z, z^2)dz$$

with $si = (sx, sy, sl)$, and θ is angle of spiral stiffeners with the longitudinal axis, d_s, d_r and d_l are the distances between stiffeners, b_s, b_r and b_l are the widths of stiffeners, μ_1 and μ_2 take the value 0 or 1, corresponding with the cases of without or with orthogonal and spiral stiffeners, respectively.

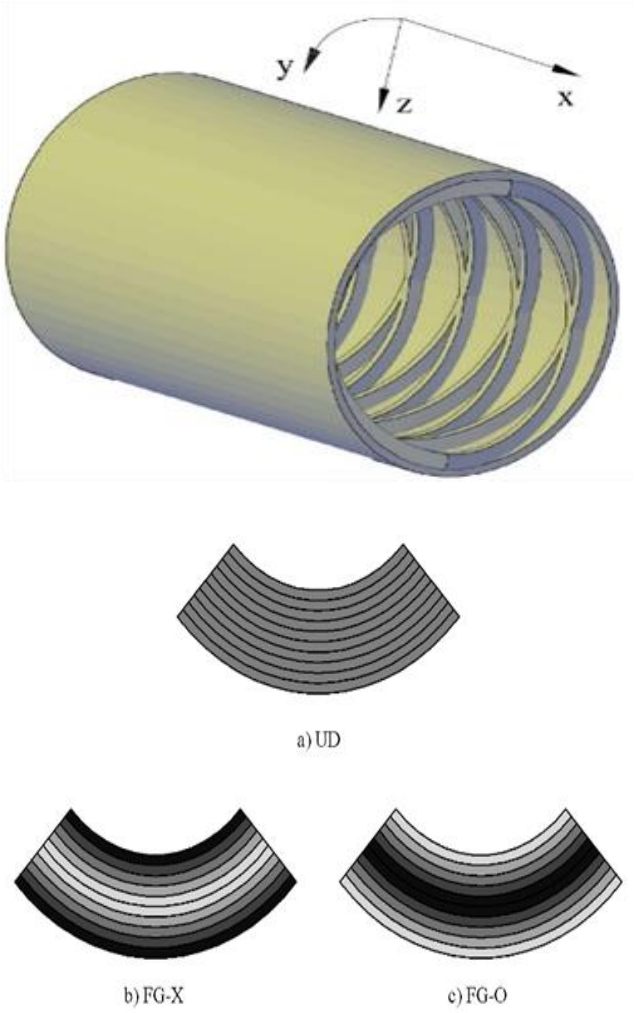

Fig 1. Configuration of the spiral stiffened cylindrical shell and graphene distribution laws of FG-GPLRC

The geometrical parameters of FG-GPLRC stiffeners are selected to let the material volume of the orthogonal stiffeners is equal to that of spiral stiffeners, i.e. the height, width and the distance between the stiffeners of the ring, stringer, and spiral stiffeners are equal. By using the simply geometrical calculation, the distance, angle, and number relation of spiral FG-GPLRC stiffeners can be obtained as $\theta = \arccos\left(n_l d_l / 2\pi R\right)$

Nonlinear equilibrium equation system of stiffened FG-GPLRC cylindrical shells based on the nonlinear Donnell shell theory can be presented as

$$\begin{aligned}
&\frac{\partial N_x}{\partial x} + \frac{\partial N_{xy}}{\partial y} = 0,\\
&\frac{\partial N_{xy}}{\partial x} + \frac{\partial N_y}{\partial y} = 0,\\
&\frac{\partial^2 M_x}{\partial x^2} + 2\frac{\partial^2 M_{xy}}{\partial x \partial y} + \frac{\partial^2 M_y}{\partial y^2} + \frac{N_y}{R}\\
&+N_x\frac{\partial^2 w}{\partial x^2} + 2N_{xy}\frac{\partial^2 w}{\partial x \partial y} + N_y\frac{\partial^2 w}{\partial y^2} = 0
\end{aligned} \tag{14}$$

The deformation compatibility equation for cylindrical shells with the geometrical nonlinearities at mid-plane can be expressed as

$$\begin{aligned}
&\varepsilon^0_{x,yy} + \varepsilon^0_{y,xx} - \gamma^0_{xy,xy} =\\
&\qquad -\frac{1}{R}w_{,xx} + w^2_{,xy} - w_{,xx}w_{,yy}
\end{aligned} \tag{15}$$

Introducing a stress function that satisfies three conditions, as

$$\begin{aligned}
N_x &= \frac{\partial^2 f}{\partial y^2},\\
N_y &= \frac{\partial^2 f}{\partial x^2},\\
N_{xy} &= -\frac{\partial^2 f}{\partial x \partial y}
\end{aligned} \tag{16}$$

Note that the first two equilibrium equations of Eq. (14) are automatically satisfied with the chosen form of stress function.

By using Eq. (16), the third equilibrium equation of Eq. (14) can be rewritten respecting the deflection and stress function

$$
\begin{aligned}
&d_{11}\frac{\partial^4 w}{\partial x^4}+d_{12}\frac{\partial^4 w}{\partial x^2\partial y^2}+d_{13}\frac{\partial^4 w}{\partial y^4}\\
&+d_{14}\frac{\partial^4 f}{\partial x^4}+d_{15}\frac{\partial^4 f}{\partial x^2\partial y^2}+d_{16}\frac{\partial^4 f}{\partial y^4}\\
&+\frac{1}{R}\frac{\partial^2 f}{\partial x^2}+\frac{\partial^2 f}{\partial y^2}\frac{\partial^2 w}{\partial x^2}\\
&+\frac{\partial^2 f}{\partial x^2}\frac{\partial^2 w}{\partial y^2}-2\frac{\partial^2 f}{\partial x\partial y}\frac{\partial^2 w}{\partial x\partial y}=0
\end{aligned}
\tag{17}
$$

The deformation compatibility equation is obtained in the new form, as

$$
\begin{aligned}
&e_{11}\frac{\partial^4 f}{\partial x^4}+e_{12}\frac{\partial^4 f}{\partial x^2\partial y^2}+e_{13}\frac{\partial^4 f}{\partial y^4}\\
&+e_{14}\frac{\partial^4 w}{\partial x^4}+e_{15}\frac{\partial^4 w}{\partial x^2\partial y^2}\\
&+e_{16}\frac{\partial^4 w}{\partial y^4}-\left(\frac{\partial^2 w}{\partial x\partial y}\right)^2\\
&+\frac{\partial^2 w}{\partial x^2}\frac{\partial^2 w}{\partial y^2}+\frac{1}{R}\frac{\partial^2 w}{\partial x^2}=0
\end{aligned}
\tag{18}
$$

The chosen solution form of deflection of shell approximately satisfies for the simply supported cylindrical shell and is suitable with the real deflection form in the case of torsional loads, presented as

$$
\begin{aligned}
w=\xi_0+\xi_1\sin\frac{m\pi x}{L}\sin\frac{n\left(y-\lambda x\right)}{R}\\
+\xi_2\sin^2\frac{m\pi x}{L}
\end{aligned}
\tag{19}
$$

where m is the number of axial half waves in x direction and n is the number of circumferential waves in y direction of shell.

By substituting the chosen solution form of deflection into the deformation compatibility equation (18), the general form of stress function is determined in the form

$$
\begin{aligned}
f=&\left(F_{11}\xi_2+F_{12}\xi_1^2\right)\cos\frac{2m\pi x}{L}\\
&+F_{21}\xi_1^2\cos\frac{2n\left(y-\lambda x\right)}{R}\\
&+\xi_1\left(F_{31}+F_{32}\xi_2\right)\cos\frac{n}{R}\left[y+\left(\frac{m\pi R}{nL}-\lambda\right)x\right]\\
&+\xi_1\left(F_{41}+F_{42}\xi_2\right)\cos\frac{n}{R}\left[y-\left(\frac{m\pi R}{nL}+\lambda\right)x\right]\\
&+F_5\xi_1\xi_2\cos\frac{n}{R}\left[y-\left(\frac{3m\pi R}{nL}+\lambda\right)x\right]\\
&+F_6\xi_1\xi_2\cos\frac{n}{R}\left[y+\left(\frac{3m\pi R}{nL}-\lambda\right)x\right]-\tau hxy
\end{aligned}
\tag{20}
$$

Introducing deflection form and stress function form into Eq. (18), and applying the Galerkin method, the equilibrium equation system is archived as

$$2\tau hn^2\lambda/R^2+U_1+U_2\xi_2+U_3\xi_1^2+U_4\xi_2^2=0, \tag{21}$$

$$U_5\xi_2+U_6\xi_1^2+U_7\xi_1^2\xi_2=0, \tag{22}$$

The circumferentially closed condition is obligatorily satisfied for the cylindrical shell as

$$\int_0^{2\pi R}\int_0^{L}\frac{\partial v}{\partial y}dxdy=0 \tag{23}$$

leads to

$$2\xi_0+\xi_2-\frac{1}{4}R\xi_1^2\frac{n}{R^2}^2=0 \tag{24}$$

The $\tau-\xi_1$ relation expression can be determined respecting the linear deflection amplitude from Eqs. (21, 22) and (24), leads to

$$
\tau=-\frac{R^2}{2hn^2\lambda}\left[\begin{aligned}
&U_1+U_2\frac{2U_6\xi_1^2}{2\left(U_5+U_7\xi_1^2\right)}+\\
&U_3\xi_1^2+U_4\left(\frac{2U_6\xi_1^2}{2\left(U_5+U_7\xi_1^2\right)}\right)^2
\end{aligned}\right]
\tag{25}
$$

The postbuckling $\tau-\xi_1$ curves of stiffened FG-GPLRC shells are investigated by using the Eq. (25). The torsional buckling load of shells can be obtained when $\xi_1\to 0$, Eq. (35) becomes

$$\tau^{upper} = -\frac{R^2}{2hn^2\lambda}U_1 \quad (26)$$

By using Eq. (26), the upper critical torsion buckling loads are determined by minimizing this equation with different modes (m,n,λ).

The maximal deflection of stiffened FG-GPLRC cylindrical shells can be archived from Eq. (19), as

$$W_{\max} = \xi_0 + \xi_1 + \xi_2 \quad (27)$$

The uniformly distributed and nonlinear deflection amplitudes ξ_0, ξ_2 can be solved from Eqs. (21) and (24) respecting ξ_1, the maximal deflection expression can be rewritten as

$$W_{\max} = \frac{\xi_1^2 n^2}{8R} + \xi_1 + \frac{2U_6\xi_1^2}{4\left(U_5 + U_7\xi_1^2\right)} \quad (28)$$

Using Eq. (25) and Eq. (28), the torsional postbuckling curves of stiffened FG-GPLRC cylindrical shells are determined in numerical form.

The twist angle can be expressed in the average form, as

$$\varphi = \frac{1}{2\pi RL}\int_0^{2\pi R}\int_0^{L}\left(\frac{\partial u}{\partial y} + \frac{\partial v}{\partial x}\right)dxdy \quad (29)$$

The explicit expression of the twist angle can be obtained after some calculations, as

$$\varphi = S_{33}^{*}\tau h + \frac{\lambda n^2\xi_1^2}{4R^2} \quad (30)$$

As can be observed, the relation between twist angle and torsional load is linear when $\xi_1 = 0$ When $\xi_0 \to 0$, $\tau - \varphi$ relation curves of shells can be determined by utilizing the combination of Eq. (28) and Eq. (30).

3. Validation, numerical investigations, and discussions

The numerical results of this present approach are compared with the results of the previous results to prove the reliability. The upper and lower torsionally critical buckling loads of cylindrical shells made of homogeneous material are compared with experimental and analytical results of Wang et al. [1], Huang and Han [4] as presented in Fig 2. As can be recognized in Fig 2, the present results agree well with the previous results.

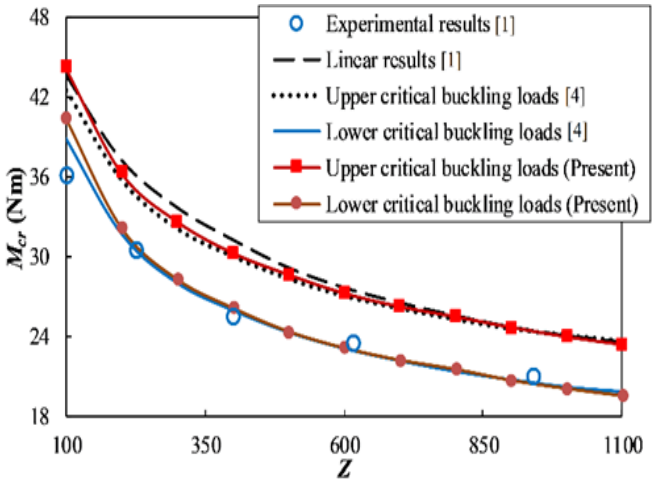

Fig 2. Comparison of critical buckling torsion of isotropic cylindrical shells

In this section, the material properties of epoxy and GPL are chosen and the material parameters applied according to the previous report [13-15]. The effects of stiffeners on the critical buckling load and postbuckling curve are investigated in three cases of unstiffened, orthogonal and spiral stiffened FG-GPLRC cylindrical shells.

In this section, the input parameters are chosen as (W = 3%, $R = 0.8m$, $L = 1.5R$, $b_r = b_s = b_l = 0.01m$, $h_r = h_s = h_l = 0.015m$, $d_r = d_s = d_l = 0.05m$, $n_r = 24$, $n_s = 100$, $n_l = 59$, $\theta = 54.06$, $m = 1$). The cases whereother input parameters are used will be annotated directly on the figures or tables.

It is illustrated in Table 1, the values of critically torsional buckling load with spiral stiffeners are the greatest and those of unstiffened shells are the smallest, respectively. These results prove that the effect of spiral stiffeners is better than that of orthogonal stiffeners on the critically torsional buckling load of FG-GPLRC cylindrical shells.

Table 1 also investigates the effects of the distribution law of graphene platelet and ratio on

the critical buckling load of shells. Critically torsional buckling loads of FG-GPLRC cylindrical shells are largest with FG-X graphene platelet distributed type and smallest with FG-O graphene platelet distributed type, respectively. ratio also strongly influences the critically torsional buckling load of shells.

Figs 3 and 4 show the effects of postbuckling curves of dimensionless deflection – torsional load and torsional angle – torsional load of unstiffened, orthogonal stiffened and spiral stiffened FG-GPLRC cylindrical shells.In general, the order of the postbuckling strengths is corresponding to the order of the critical loads, however, there can be some anomalies when the deflection is large enough. Effects of R/h ratio on the dimensionless deflection – torsional load and torsional angle – torsional load postbuckling curves of FG-GPLRC cylindrical shells are investigated in Figs 5 and 6. Clearly, the R/h ratio of shells largely influences the postbuckling behavior of shells. Due to the complex behavior of FG-GPLRC cylindrical shells, the irregular changes on the trend of the postbuckling curve are obtained when the R/h ratio varies. In addition, the snap-through phenomenon increases when the R/h ratio increases.

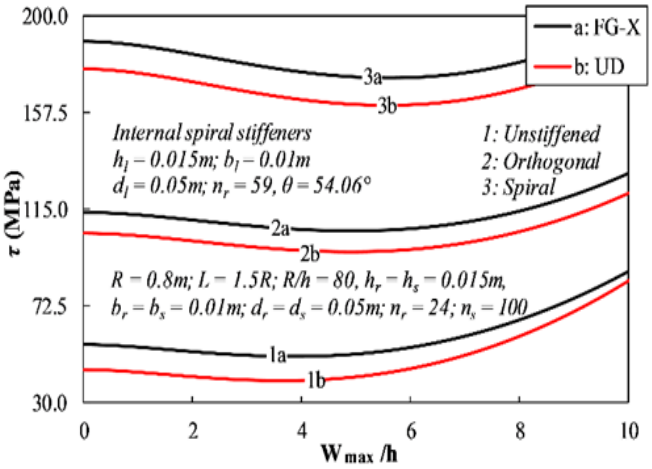

Fig 3. Comparison of dimensionless deflection – torsional load postbuckling curves of unstiffened, orthogonal stiffened and spiral stiffened FG-GPLRC cylindrical shells

Table 1. The critically torsional buckling loads (MPa) of unstiffened, orthogonal stiffened and spiral stiffened FG-GPLRC cylindrical shells

	Distribution law	Unstiffener	Orthogonal stiffener	Spiral stiffener
$R/h=60$	UD	64.54 (7;0.45)[a]	116.72 (6;0.59)	183.65 (6;0.50;59;54.06)[b]
	FG-X	79.80 (7;0.49)	130.54 (6;0.60)	199.38 (6;0.51;59;54.06)
	FG-O	47.21 (8;0.44)	103.92 (6;0.59)	169.30 (6;0.48;59;54.06)
$R/h=70$	UD	53.16 (8;0.46)	108.96 (6;0.59)	178.64 (6;0.48;59;54.06)
	FG-X	65.73 (7;0.46)	120.16 (6;0.60)	192.02 (6;0.50;59;54.06)
	FG-O	39.14 (8;0.41)	98.71 (6;0.59)	166.61 (6;0.47;59;54.06)
$R/h=80$	UD	44.78 (8;0.43)	104.26 (6;0.59)	176.88 (6;0.47;59;54.06)
	FG-X	55.75 (8;0.47)	113.88 (6;0.60)	188.95 (6;0.48;59;54.06)
	FG-O	33.00 (9;0.42)	95.55 (6;0.59)	166.14 (6;0.46;59;54.06)

[a] the numbers in the brackets show the critical mode for unstiffened and orthogonal stiffened cases (*n;* λ).
[b] the numbers in the brackets show the critical mode for spiral stiffener case (*n;* λ).

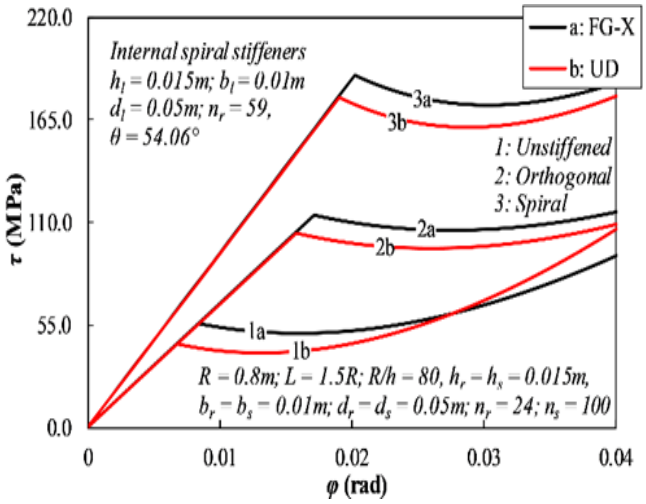

Fig 4. Comparison of torsional angle – torsional load postbuckling curves of unstiffened, orthogonal stiffened and spiral stiffened shells

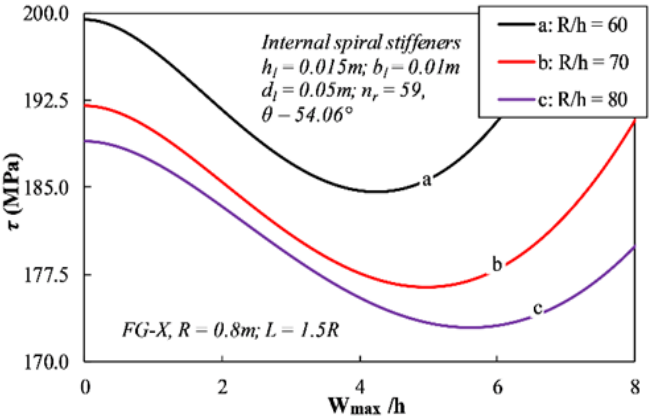

Fig 5. Comparison of dimensionless deflection – torsional load postbuckling curves spiral stiffened FG-GPLRC shells with different R/h ratios

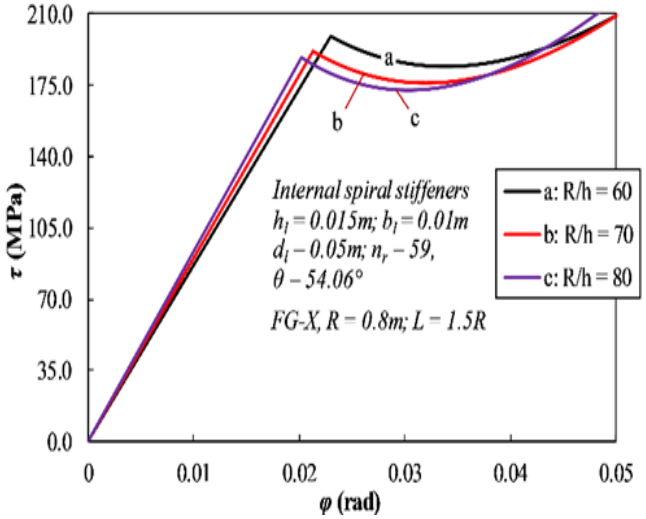

Fig 6. Comparison of torsional angle – torsional load postbuckling curves of unstiffened, orthogonal stiffened and spiral stiffened FG-GPLRC cylindrical shells with different R/h ratios

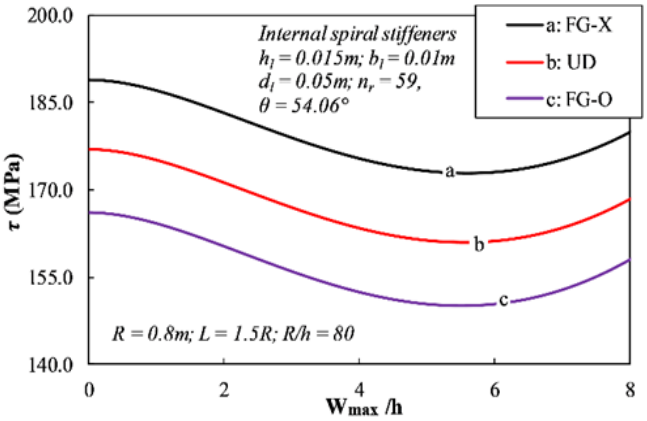

Fig 7. Comparison of dimensionless deflection – torsional load postbuckling curves of spiral stiffened FG-GPLRC cylindrical shells with different distribution laws of graphene platelet

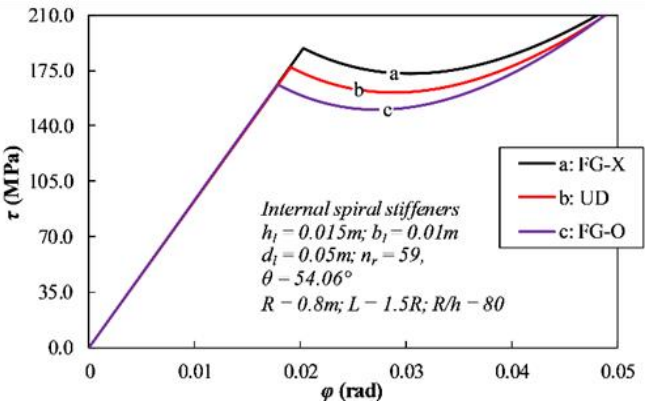

Fig 8. Comparison of torsional angle – torsional load postbuckling curves of spiral stiffened FG-GPLRC cylindrical shells with different distribution laws of graphene platelet

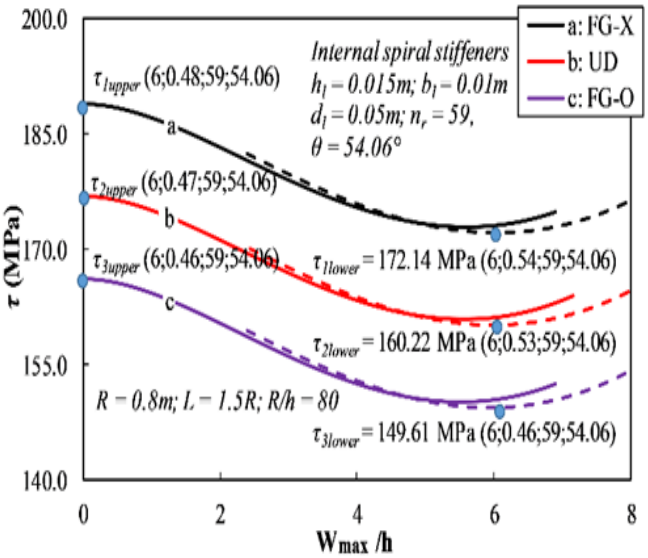

Fig 9. Upper and lower critical buckling load at the dimensionless deflection – torsional load postbuckling curves of spiral stiffened FG-GPLRC cylindrical shells

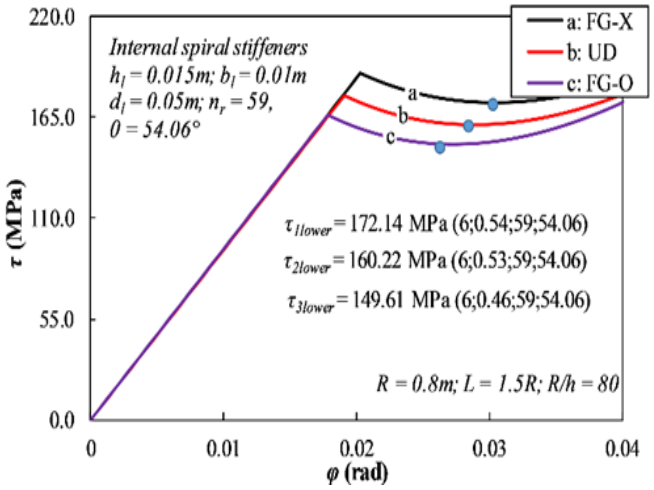

Fig 10. Upper and lower critical buckling load at the torsional angle – torsional load postbuckling curves of spiral stiffened FG-GPLRC cylindrical shells

Comparisons of dimensionless deflection–torsional load and torsional angle–torsional load postbuckling curves of spiral stiffened FG-GPLRC cylindrical shells with different distribution laws of graphene platelet are shown in Figs 7 and 8. As can be seen, the regular trends of postbuckling behavior for three distribution laws of graphene platelet are observed in these investigations. The comparison of lower and upper torsional buckling loads is presented in Figs 9 and 10. As can be seen, the different torsional buckling modes are obtained for the upper and lower critical buckling load of the shell. Additionally, the obtained results show that the significant differences between upper and lower critically torsional buckling loads are presented in all investigations.

A developed Lekhnitskii's smeared stiffener technique is applied for three types of graphene platelet distributed laws of FG-GPLRC cylindrical shell in this paper. The cylindrical shells are reinforced by ring, stringer and spiral FG-GPLRC stiffeners attached to the inside of the shells. Some remarks are deduced from numerical investigations of the present study as follow:

4. Conclusion

a) The effect of spiral FG-GPLRC stiffeners on the torsional critical buckling load is much larger than one of the orthogonal FG-GPLRC stiffeners.

b) FG-X types are the most effective on critical buckling load of FG-GPLRC shells in all graphene distributed laws. Contrary, critical buckling loads of the FG-O shell are the smallest.

c) As a final remark, geometrical parameters strongly influence the nonlinear buckling behavior of FG-GPLRC cylindrical shells subjected to torsional load.

Acknowledgments

This research is funded by University of Transport Technology (UTT) under grant number DTTD2021-03.

References

[1] D.Y. Wang, H.W. Ma, G.T. Yang. (1992). Studies on the torsional buckling of elastic cylindrical shells. Appl Math Mech, 13, 211–215.

[2] A.H. Sofiyev, E. Schnack. (2004). The stability of functionally graded cylindrical shells under linearly increasing dynamic torsional loading. Eng Struct, 26(10), 1321–1331.

[3] H.S. Shen. (2009). Torsional buckling and postbuckling of FGM cylindrical shells in thermal environments. Int J Non Linear Mech, 44(6), 644–657.

[4] H. Huang, Q. Han. (2010). Nonlinear buckling of torsion – loaded functionally graded cylindrical shells in thermal environment. Eur J Mech A/Solids, 29(1), 42–48.

[5] A.M. Najafov, A.H. Sofiyev, N. Kuruoglu. (2013). Torsional vibration and stability of functionally graded orthotropic cylindrical shells on elastic foundations. Meccanica, 48, 829–840.

[6] D.V. Dung, L.K. Hoa. (2015). Nonlinear torsional buckling and postbuckling of eccentrically stiffened FGM cylindrical shells in thermal environment. Compos Part B Eng, 69, 378–388.

[7] V.H. Nam, N.T. Trung, L.K. Hoa. (2019). Buckling and postbuckling of porous cylindrical shells with functionally graded

composite coating under torsion in thermal environment. Thin Wall Struct, 144, 106253

[8] N.T. Phuong, D.T. Luan, V.H. Nam, P.T. Hieu. (2019). Nonlinear approach on torsional buckling and postbuckling of functionally graded cylindrical shells reinforced by orthogonal and spiral stiffeners in thermal environment. Proc Inst Mech Eng C: J Mech Engin Sci, 233(6), 2091–2106.

[9] V.H. Nam, N.T. Phuong, K.V. Minh, P.T. Hieu. (2018). Nonlinear thermo-mechanical buckling and post-buckling of multilayer FGM cylindrical shell reinforced by spiral stiffeners surrounded by elastic foundation subjected to torsional loads. Eur J Mech A/Solids, 72, 393–406.

[10] V.H. Nam, N.T. Phuong, N.T. Trung. (2019). Nonlinear buckling and postbuckling of sandwich FGM cylindrical shells reinforced by spiral stiffeners under torsion loads in thermal environment. Acta Mech, 230, 3183–3204.

[11] N.T. Phuong, V.H. Nam, N.T. Trung, V.M. Duc, P.V. Phong. (2019). Nonlinear stability of sandwich functionally graded cylindrical shells with stiffeners under axial compression in thermal environment. Int J Struct Stab Dyn, 19(07), 1950073.

[12] N.T. Phuong, V.H. Nam, N.T. Trung, V.M. Duc, N.V. Loi, N.D. Thinh, P.T. Tu. (2019). Thermomechanical postbuckling of functionally graded graphene-reinforced composite laminated toroidal shell segments surrounded by Pasternak's elastic foundation. Journal of Thermoplastic Compos Mater, DOI: 10.1177/0892705719870593

[13] M. Song, J. Yang, S. Kitipornchai. (2018). Bending and buckling analyses of functionally graded polymer composite plates reinforced with graphene nanoplatelets. Compos Part B, 134, 106–113.

[14] M. Song, X. Li, S. Kitipornchai, Q. Bi, J. Yang. (2019). Low-velocity impact response of geometrically nonlinear functionally graded graphene platelet-reinforced nanocomposite plates. Nonlinear Dyn, 95(3), 2333–2352.

[15] H. Wu, S. Kitipornchai, J. Yang. (2017). Thermal buckling and postbuckling of functionally graded graphene nanocomposite plates. Mater Des, 132, 430–441.